Progress In Electromagnetics Research, Vol. 144, 221–228, 2014

Partial Discharge Detection Approach for a Medium Voltage Switchgear System

ZhuoLun Cai, Richardt H. Wilkinson*, and Alexe Bojovschi

Abstract—Partial Discharge detection techniques strive to ensure a safe and reliable power network by preventing power failure. In this work, electromagnetic sensing of partial discharge, in air-insulated medium voltage switchgear (Type D24-121114 of Driescher) is considered. The partial discharges are approximated by Gaussian sources. A versatile broadband sensor for detecting two major types of partial discharge was designed and optimized. The antenna has low return loss and high gain over the frequency band of corona discharge, 0.75–0.9 GHz and dry band arcing, 1.25–1.4 GHz. The horn antenna is incorporated into the medium voltage switchgear for detecting partial discharges. The analysis of the electromagnetic field distributions generated by partial discharges in switchgear is coupled with the sensing efficiency of the horn antenna. The results indicate a good correlation between the intensity, location and frequency band of partial discharge and their sensing. This study provides the foundation for a dual band detection system of partial discharge in switchgear systems.

1. INTRODUCTION

Erosive discharges, also called Partial Discharges (PD), can occur in the form of cavity discharges and surface discharges. PD is widely present within the electrical insulation of power networks, transformers, switchgear systems, cables and windings in large motors and generators [1, 2]. These types of discharges can lead to dielectric breakdowns and failures of high voltage components. To prevent these types of events in switchgear systems, PD monitoring is essential. Detecting electromagnetic (EM) radiation of PD in the ultra high frequency (UHF) band becomes one of the most widely used measurement techniques in the world [3–5]. UHF PD detection methods can overcome known drawbacks of other classical PD measurements, such as 'high voltage on site commissioning tests on gas-insulated substations' [6]. The UHF method is used to detect PD signals in the 0.3 GHz to 3 GHz band due to its lower level of noise compared to lower frequency bands used previously. The history of employing an antenna as a UHF sensor for PD detection can be traced back to the middle 1990s [7, 8]. The technology has recently been used for PD online monitoring [5, 9] and PD detection in systems such as sulfur hexafluoride (SF6) insulated switchgears [10, 11] and gas-insulated substations [12].

There are many different types of PD in high voltage devices [13–16]. However, the most common types are corona discharge and dry band discharge. The increase in hydrophilic degree of insulator surfaces, facilitates dry band arcing. The dry band arcing is responsible for a significant amount of current flowing on the surface of insulators enhancing the likelihood of insulator failure [17, 18]. Previous measurements used methods such as leakage current and PD detection to characterize the condition of insulators and hence to detect dry band discharges [14, 19, 20]. The likelihood of corona discharges on insulator surfaces and their transition to dry band arching was also studied using PD [21].

The spectra in which these discharges emit, are predominantly the 0.8 GHz to 0.9 GHz band, and the 1.25 GHz to 1.4 GHz band [14]. These wide frequency bands indicate a need for a broadband sensor for detection. Some sensors, like monopole antennas and patch antennas, are commonly used to detect

Received 21 October 2013, Accepted 9 January 2014, Scheduled 22 January 2014
* Corresponding author: Richardt Wilkinson (richardt.wilkinson@rmit.edu.au).
The authors are with the School of Electrical and Computer Engineering, RMIT University, Melbourne, VIC 3001, Australia.

PD. Horn antennas, as those commonly used for radar systems [22], can be optimized for PD detection. Furthermore, horn antennas can ensure high gain, broader bandwidth and ease of manufacturing.

This work proposes a dual band antenna for detecting two types of PD in an air-insulated medium voltage switchgear (AIS) system. The design and optimization of the PD sensor is detailed. The efficiency of the antenna for detecting PD in AIS is also investigated. The distribution of the electric fields generated by the partial discharges simulated on the surfaces of insulators are analyzed. The radiative coupling of PD signals to the horn antenna is also examined.

2. COMPUTATIONAL APPROACH

The design and optimization of the sensors and the study of the interaction of electromagnetic radiation from PD, with different components in AIS, were investigated using a Finite Element Method (FEM) [23–26], as implemented in ANSYS® High Frequency Structure Simulator (HFSS) [27] package.

In this work, the FEM relies on an integral formulation of the variational boundary value problem [28]. In this method the volume of interest is subdivided in surface or volume elements where the unknown function is approximated as a polynomial. An adaptive meshing is used in the calculations. In this manner the finite element mesh is created and automatically refined in the areas of highest error. This allows for increasing the accuracy of the succeeding adaptive solution.

The intensity of the field over the radiation surface is used to calculate the field surrounding the sensor. The space surrounding the antenna is divided into two domains: the near-field region and the far-field region. The electric field $\mathbf{E}(x, y, z)$ external to a region bounded by a closed surface may be written as follows:

$$E(x,y,z) = \int_S \left(\langle j\omega\mu_0 H_{\tan}\rangle G + \langle E_{\tan} \times \nabla G\rangle + \langle E_{normal} \times \nabla G\rangle\right) dS \tag{1}$$

In (1), S is the radiation boundary surface, μ_0 the relative permeability of air, $H_{\tan}$ the component of the magnetic field that is tangential to the surface, E_{normal} the component of the electric field that is normal to the surface, $E_{\tan}$ the component of the electric field that is tangential to the surface, and $G = (e^{-jk_0}|\mathbf{r} - \mathbf{r}_0|\sqrt{\mu_r\varepsilon_r})/|\mathbf{r} - \mathbf{r}_0|$ the Green's function in free space. In this function, $k_0 = \omega\sqrt{\mu_0\varepsilon_0}$ is the free space wave number, $\mathbf{r}$ and $\mathbf{r}_0$ are field points and source points on the integrated surface, $\varepsilon_0 = 1/c^2\mu_0$ is the permittivity of the free space, ε_r is the relative permittivity of copper used for the antenna and μ_r is its relative permeability.

The designs of ultra-wide-band horn antennas were detailed previously [29, 30]. Those designs refer to frequencies above 1.5 GHz. The available horn antennas are not suitable for PD detection in the frequency range from 0.7 to 1.4 GHz. However, they are a good foundation for the present study and antenna design. The cut-off frequency, which is proportional to the dimensions of the waveguide of the horn antenna, should have a lower value to ensure small return losses in the required frequency band.

The double-ridged horn antenna was designed for PD detection. The model of the optimized double-ridged horn antenna together with the main components is presented in Figure 1. The antenna was surrounded by an air radiation boundary condition to absorb all the outgoing radiation. In this way, radiation is prevented from reflecting back to the antenna and used to estimate the far-field radiation pattern.

The horn antenna was fed through a wave port, which was excited by a pin feed that creates the electric field in the antenna. The feed is the communication point between the coaxial cable and waveguide of the horn. A standard 50 Ω coaxial cable with inner and outer conductor radii of 1.3 and 3 mm respectively, is considered to feed the horn antenna. All the antenna parameters including the feed, waveguide, taper and ridge were optimised for dual working frequency bands of 0.75 to 0.9 GHz and 1.25 to 1.4 GHz.

It is indicated in [31] that the ratio between the dimensions of the rectangular waveguide cross-section of the double-ridged horn is 2 : 1. After optimization in HFSS, the final small aperture is computed to be 160 mm × 74 mm, as seen in Figure 1. The optimum length of the waveguide section was calculated as 37 mm. Figure 1 also shows the dimensions of the ridge section. The ridge design is calculated in agreement with the pin feed and the frequency band. The height of the feeding pin is equal to 2 mm.

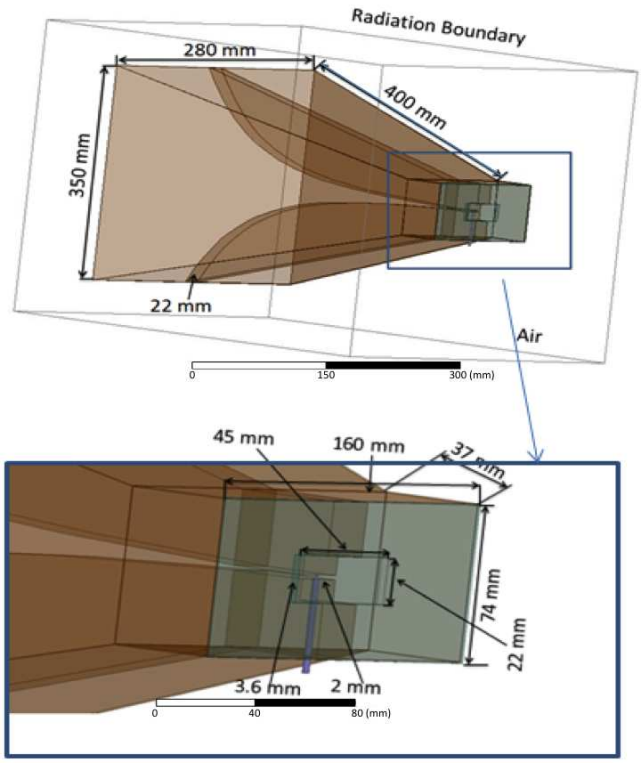

Figure 1. Structural representation of the optimized double-ridged horn antenna surrounded by air and bound by radiation boundary conditions.

The length of the horn is normally larger than $\lambda/2$, where λ is the wavelength of the frequency of interest. Therefore, the total calculated length for the present case should be larger than 350 mm. After optimization in HFSS, a length of 412 mm was obtained. When the larger aperture dimensions of the horn are 350 mm × 280 mm, the performance of the double-ridged horn achieves the desired bandwidth and gain requirements. Detailed design of the tapering of the ridges is based on results published previously [31]. The exponential tapering of the ridges after optimization in HFSS is described by the following equation:

$$y = 0.001\left(e^{-0.01301t} + 0.02t\right) \tag{2}$$

where t is the dimension of the air gap between the two ridges. The thickness of the taper is 22 mm.

The reflection coefficients were calculated for different parametric sweeps of the structural dimensions used to optimize the horn antenna. The error tolerance of the sweep calculations was set to 0.5% and a maximum of 250 solutions were considered for the interpolation sweep.

HFSS was also used to simulate the medium voltage switchgear system (Type D 24 — 121114 of Driescher — Compact Switchgears 24 kV) [32] with the horn antenna inside, used for PD detection. All components of this type of switchgear have been incorporated into the simulation model (Figure 2), including voltage transformer, current transformer, spherical terminal studs, fuse disconnectors, HV-HBC fuse, earthing switch and all connection parts such as nails. The metallic enclosure of the switchgear has a length of 1192 mm, a height of 1353 mm and a width of 1094 mm.

The PD source is simulated numerically in the AIS by a Gaussian pulse [25] with a center frequency of 800 MHz and a bandwidth of 200 MHz. The radius ($\mathbf{r}_0$) of the Gaussian beam width is 100 mm, which corresponds with the size of the surface PD. The amplitude of the Gaussian source is 1 V/m and it is set to propagate in the x direction. For further study the central frequency is changed to 1.3 GHz in order to detect dry band discharge arcing emitted at this frequency. All the other parameters are kept the same as when a center frequency of 800 MHz is used. Five PD locations were considered for analysis in the AIS.

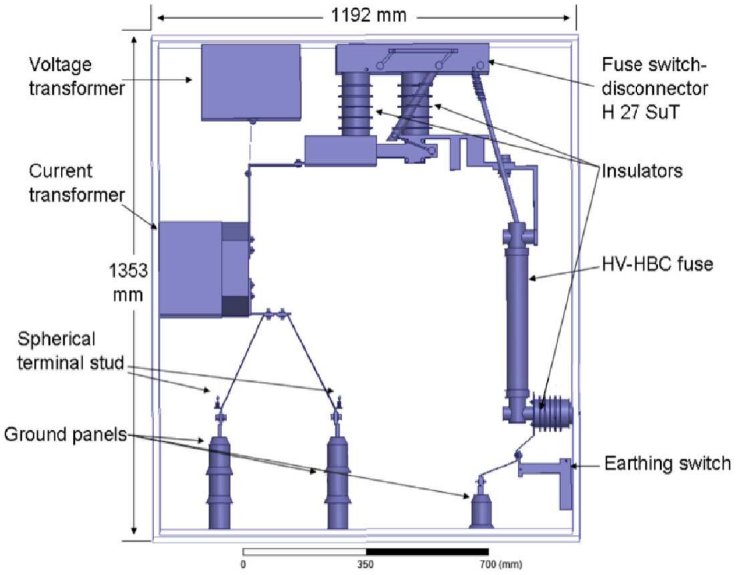

Figure 2. Schematical representation of the simulated system (Type D 24 — 121114 of Driescher — Compact Switchgears 24 kV) providing a front view. (Redrawn from [33]).

3. RESULTS AND DISCUSSIONS

The return loss (S_{11}) result for the optimized double-ridged horn is presented in Figure 3. From the figure, it can be seen that the double-ridged horn antenna is suitable for the two frequency bands of interest. The spectra correspond to two frequency bands: e.g., corona discharge (0.75 GHz–0.9 GHz) and dry band arcing (1.25 GHz–1.4 GHz) respectively. The advantage of the ridged-horn antenna is predominantly its smaller size compared to an equivalent conical horn antenna for the same frequency and bandwidth requirements. Figure 3 shows that from about 0.75 GHz to about 1.4 GHz, S_{11} has smaller values, which are predominantly below −10 dB.

To assess the efficiency of the antenna, the realized gain was calculated. Representative E-plane radiation patterns and the realized gain at 0.8 GHz and 1.3 GHz, for $\phi = 90°$ are presented in Figure 4. The peak gains at 0.8 GHz and 1.3 GHz are 8.53 dBi and 10.20 dBi respectively.

The distribution of the electric field in AIS and the coupled electric field to the horn antenna for

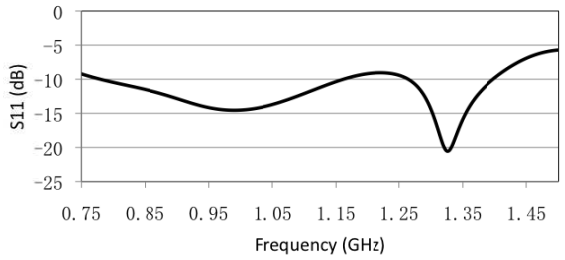

Figure 3. Optimum values of the return loss (S_{11}) of the double-ridged horn antenna designed for detecting corona and dry band arcing.

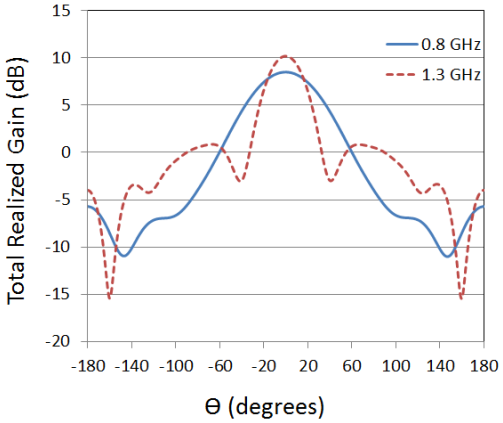

Figure 4. E-plane total realized gain of the double-ridged horn antenna at working frequency of 0.8 GHz and 1.3 GHz for $\phi = 90°$.

zero phases of a PD source are shown in Figures 5 and 6, respectively. The amplitude of the PD source E_0 and the propagation direction in the x direction is shown in these figures. The maximum value of the E-field coupled to the horn antenna for an 800 MHz center frequency of the PD discharge is 67.107 V/m (Figure 5). In Figure 6, a maximum value of 2.347 V/m is found for a center frequency of 1.3 GHz. It should be noted that in switchgear the E-field is presented with a transparent mode to increase the visibility of its components. In Figures 5 and 6, Reference PD corresponds to PD location 1 in Figure 7. PD2 through PD5 correspond to PD locations 2 to 5 in Figure 7.

The maximum value of the electric field when the PD is located at five different locations in the AIS is shown in Figure 7. From the figure it can be seen that the detection of the PD location and its amplitude is feasible. This is more evident for frequencies around 800 MHz, which are dominant for PD activity in the power network. The unexpected amplitudes for frequencies higher than 0.9 GHz are due to multi-path phenomena, which are expected in enclosed systems such as AIS.

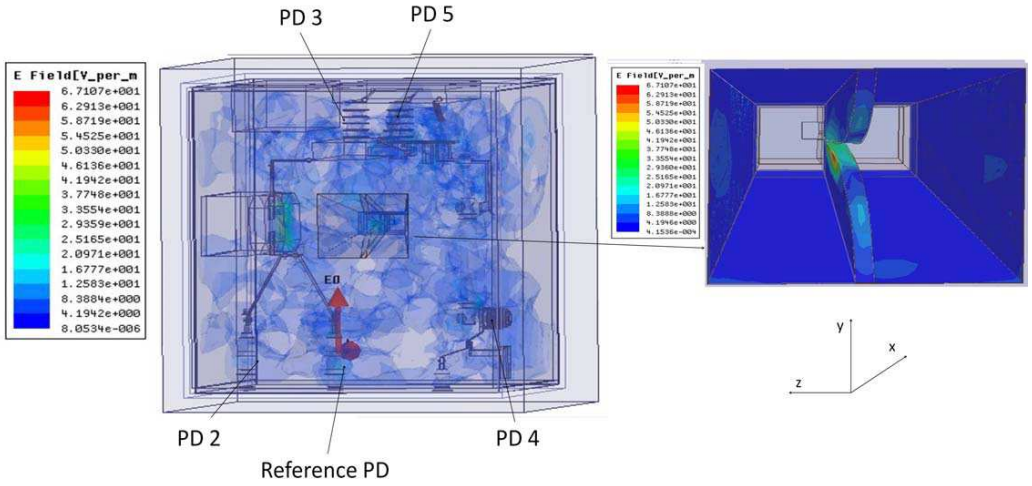

Figure 5. The E field distribution in the AIS and the E-field coupled to the double-ridged horn antenna for a PD with an 800 MHz center frequency.

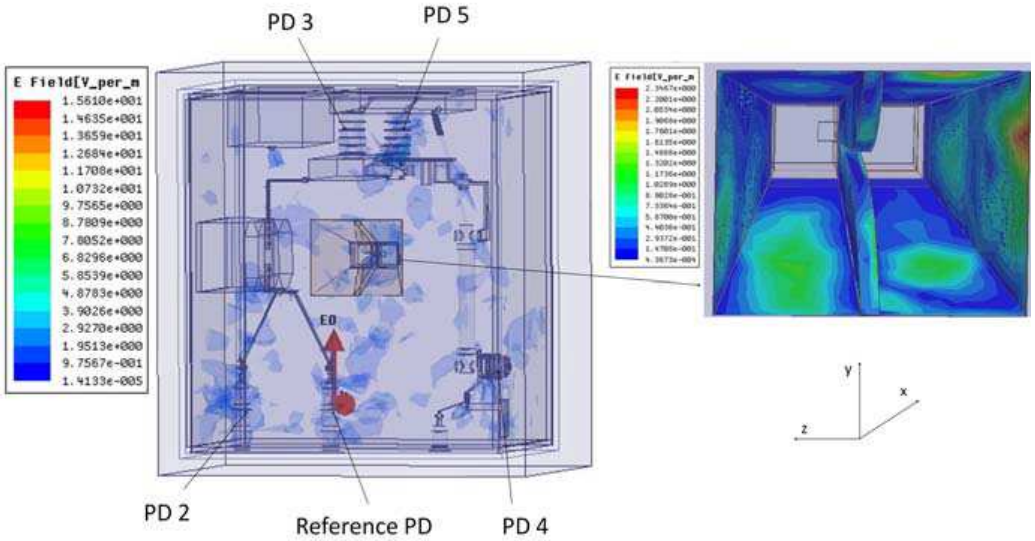

Figure 6. The E-field distribution in the AIS and the E-field coupled to the double-ridged horn antenna for a PD with a 1.3 GHz center frequency.

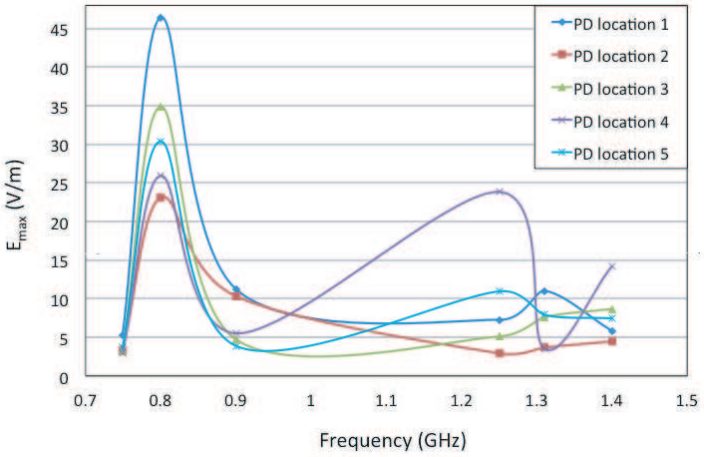

Figure 7. Maximum amplitude of the electric field detected by horn antenna for PD located at five different locations.

4. CONCLUSION

The paper presents the optimized geometrical and electromagnetic characteristics of a double-ridged horn antenna for PD detection in the 0.75 to 0.9 GHz and 1.25 to 1.4 GHz bands. Furthermore, the antenna is used to sense spatially distributed PD in the AIS. The results highlight the potential use of a double-ridged horn antenna for PD detection in AIS.

ACKNOWLEDGMENT

The authors acknowledge Dr. Hubert Schlapp from SebaKMT Germany for providing the scientific interest in this topic and for technical documentation. The authors would like to acknowledge the technical support provided by Mr. Thomas Benke from ANSYS Australia.

REFERENCES

1. Bargigia, A., W. Koltunowicz, and A. Pigini, "Detection of parallel discharges in gas insulated substations," *IEEE Transactions on Power Delivery*, Vol. 7, No. 3, 1239–1249, 1992.
2. Al Murawwi, E., K. Al Mazam, A. R. Huwair, A. El-Hag, and N. Qaddoumi, "Partial discharge and oil quality monitoring using an RF antenna," *IEEE Industry Applications Magazine*, Vol. 16, No. 3, 57–59, 2010.
3. Hikita, M., S. Ohtsuka, and S. Matsumoto, "Recent trend of partial discharge measurement technique using UHF electromagnetic wave detection method," *IEEJ Transactions on Electrical and Electronic Engineering*, Vol. 2, No. 5, 504–509, 2007.
4. Judd, M. D., L. Yang, and I. B. B. Hunter, "Partial discharge monitoring of power transformers using UHF sensors. Part I: Sensors and signal interpretation," *IEEE Electrical Insulation Magazine*, Vol. 21, No. 2, 5–14, 2005.
5. Wong, K. L. and A. Bojovschi, International Patent, WO/2013/091028, Jun. 27, 2013.
6. Bell, R., C. Charlson, S. P. Halliday, T. Irwin, J. Lopez-Roldan, and J. Nixon, "High-voltage onsite commissioning tests for gas-insulated substations using UHF partial discharge detection," *IEEE Transactions on Power Delivery*, Vol. 18, No. 4, 1187–1191, 2003.

7. Sun, Y., H. Yin, Q. Zhang, F. Yu, H. Wang, and Y. Qiu, "Partial discharge detection for GIS using narrow band ultra-high-frequency (UHF) method," *Proceedings of the International Symposium on Electrical Insulating Materials*, Vol. 3, 748–751, 2005.
8. Miyata, T. and H. Otani, "Microwave sensor for detecting a discharge occurring in an electrical apparatus," US Patent No. 5726576, 1998.
9. Shibuya, Y., S. Matsumoto, M. Tanaka, H. Muto, and Y. Kaneda, "Electromagnetic waves from partial discharges and their detection using patch antenna," *IEEE Transactions on Dielectrics and Electrical Insulation*, Vol. 17, No. 3, 862–871, 2010.
10. Tsurimoto, T., M. Yoshimura, H. Muto, and M. Arioka, "Partial discharge monitoring system for cubicle type GIS," *Proc. of Int. Conf. on Condition Monitoring and Diagnosis*, 432–436, 2008.
11. De Kock, N., B. Coric, and R. Pietsch, "UHF PD detection in gas-insulated switchgear — Suitability and sensitivity of the UHF method in comparison with the IEC 270 method," *IEEE Electrical Insulation Magazine*, Vol. 12, No. 6, 20–26, 1996.
12. Kurrer, R. and K. Feser, "The application of ultra-high-frequency partial discharge measurements to gas-insulated substations," *IEEE Transactions on Power Delivery*, Vol. 13, No. 3, 777–782, 1998.
13. Chatpattananan, V., "Linear discriminant analysis for partial discharge classification on high voltage equipment," *Proc. of IEEE Conference on Electrical Insulation and Dielectric Phenomena*, 627–630, Oct. 2006.
14. Fernando, S. C., K. L. Wong, and W. S. T. Rowe, "Detection of corona and dry-band arc discharges on nano-composite epoxy insulators using RF sensing," *Progress In Electromagnetics Research*, Vol. 125, 237–254, 2012.
15. Bojovschi, A., W. R. Rowe, and K. L. Wong, "Electromagnetic field intensity generated by partial discharge in high voltage insulating materials," *Progress In Electromagnetics Research*, Vol. 104, 167–182, 2010.
16. Bojovschi, A., K. L. Wong, and W. S. T. Rowe, "The influence of hanging water droplets on discharge activity, application to high voltage insulators," *Applied Physics Letters*, Vol. 98, No. 9, 091504-1–091504-3, 2011.
17. Gorus, R. S., E. A. Cherney, and R. Hackam, "The AC and DC performance of polymeric insulating materials under accelerated aging in a fog chamber," *IEEE Transactions on Power Delivery*, Vol. 3, No. 4, 1892–1902, 1988.
18. Meyer, L. H., S. H. Jayaram, and E. A. Cherney, "Correlation of damage, dry band arcing energy, and temperature in inclined plane testing of silicone rubber for outdoor insulation," *IEEE Transactions on Dielectrics and Electrical Insulation*, Vol. 11, No. 3, 424–432, 2004.
19. El-Hag, A. H., "Leakage current characterization for estimating the conditions of non-ceramic insulators' surfaces," *Electric Power Systems Research*, Vol. 77, 379–384, 2007.
20. Kumagai, S. and N. Yoshimura, "Leakage current characterization for estimating the conditions of ceramic and polymeric insulating surfaces," *IEEE Transactions on Dielectrics and Electrical Insulation*, Vol. 11, No. 4, 681–690, 2004.
21. Lopes, I. J. S., S. H. Jayaram, and E. A. Cherney, "A method for detecting the transition from corona from water droplets to dry-band arcing on silicone rubber insulators," *IEEE Transactions on Dielectrics and Electrical Insulation*, Vol. 9, No. 6, 964–971, 2002.
22. Kampeephat, S., P. Krachodnok, and R. Wongsan, "High-gain and light-weight antenna for radar system using a horn covered with curved woodpile EBG," *PIERS Proceedings*, 1628–1630, Kuala Lumpur, Malaysia, Mar. 27–30, 2012.
23. Zienkiewicz, O. C. and R. L. Taylor, *The Finite Element Method: Solid Mechanics, Volume 2*, 5th Edition, Elsevier, Oxford, 2000.
24. Csendes, Z. J. and P. Silvester, "Numerical solution of dielectric loaded waveguides: I — Finite-element analysis," *IEEE Transactions on Microwave Theory and Techniques*, Vol. 18, No. 12, 1124–1131, 1970.
25. Daly, P., "Hybrid-mode analysis of microstrip by finite-element methods," *IEEE Transactions on Microwave Theory and Techniques*, Vol. 19, No. 1, 19–25, 1971.

26. Saad, S. M., "Review of numerical methods for the analysis of arbitrarily-shaped microwave and optical dielectric waveguides," *IEEE Transactions on Microwave Theory and Techniques*, Vol. 33, No. 10, 894–899, 1985.
27. ANSYS® HFSS, Release 13.0, ANSYS, Inc., USA, 2010.
28. Davidson, D. B., *Computational Electromagnetics for RF and Microwave Engineering*, Cambridge, 2005.
29. Shin, J., W. Lee, J. Kim, D. Choi, J. So, W. Jang, I. Han, and C. Cheon, "Design of attenuated horn antenna to receive high power pulse," *Proceedings of IEEE Antennas and Propagation Society International Symposium*, 625–628, Jun. 9–15, 2007.
30. Qiu, J., Y. Suo, and W. Li, "Research and design on ultra-wideband dielectric hemispheric lens loaded quad-ridged horn antenna," *Proceedings of International Conference on Antenna Theory and Techniques*, 253–255, Sept. 17–21, 2007.
31. Xiu, M., "Design and simulation of 500 MHz–2 GHz high performance double-ridged antenna," *Electronic Measurement Technology*, Vol. 30, No. 11, 78–82, 2007.
32. Zheng, B. and A. Bojovschi, "Electromagnetic sensing of partial discharge in air-insulated medium voltage switchgear," *PIERS Proceedings*, 1363–1366, Moscow, Russia, Aug. 19–23, 2012.
33. Driescher, "Air-insulated medium-voltage compact switchgears for substations," Dec. 20, 2013, [Online]. Available: http://www.driescher.com/products/788e.pdf.